PCCP

Accepted Manuscript

This is an *Accepted Manuscript*, which has been through the Royal Society of Chemistry peer review process and has been accepted for publication.

Accepted Manuscripts are published online shortly after acceptance, before technical editing, formatting and proof reading. Using this free service, authors can make their results available to the community, in citable form, before we publish the edited article. We will replace this *Accepted Manuscript* with the edited and formatted *Advance Article* as soon as it is available.

You can find more information about *Accepted Manuscripts* in the **Information for Authors**.

Please note that technical editing may introduce minor changes to the text and/or graphics, which may alter content. The journal's standard **Terms & Conditions** and the **Ethical guidelines** still apply. In no event shall the Royal Society of Chemistry be held responsible for any errors or omissions in this *Accepted Manuscript* or any consequences arising from the use of any information it contains.

www.rsc.org/pccp

PCCP

ARTICLE

Doxycycline and Oxytetracycline Loading of a Zwitterionic Amphoteric Surfactant-Gel and their Controlled Release.

A. Cesaretti,[a] B. Carlotti,[a] P. L. Gentili,[a] C. Clementi,[a] R. Germani[a] and F. Elisei[a]

Oxytetracycline (OX) and Doxycycline (DX) are antibiotics belonging to the family of tetracyclines. We present a UV-Visible steady state and time-resolved experimental study of OX and DX and their biologically active Mg^{2+} complexes loaded within a hydrogel matrix. Hydrogels are a three dimensional network of worm-like micelles, mutually intertwined, forming a pattern of hydrophobic domains and water pools. We resorted to a hydrogel, made of a zwitterionic N-oxide surfactant (*p*-dodecyloxybenzyldimethylamine N-oxide, *p*DoAO), which showed promising features as drug vehicle. The spectral and photophysical properties of the drugs are significantly altered by the inclusion in the hydrophobic domains of the gel and these variations are indicators of the permeation ratio of the drug in between the micelles forming the gel network. We thus get a clear picture of the distribution of the drug molecules and metal chelates into the two different kinds of environment, where the hydrophobic domains are also able to cause a gel-induced deprotonation of these two drugs. Furthermore, the amphoteric nature of the surfactant is responsible for its peculiar acid-base behaviour: under acidic pH conditions, the surfactant gets protonated and the stability of the gel network is damaged. This feature can be thus exploited for the pH controlled release of the tetracycline drugs.

Introduction

Hydrogels are micro-heterogeneous systems used, among other applications, as drug vehicles. This purpose is promoted by their biocompatibility with human tissues (due to the high water content) and their malleability.[1,2] Hydrogels are complex networks of covalent and non-covalent nanostructures (such as polymer chains, peptide-based supramolecular structures or micellar aggregates) made up of hydrophobic and hydrophilic domains. Under specific experimental conditions ranging from pH to temperature, from electrostatic to hydrophobic interactions, polymer molecules, peptide or micellar aggregates can interact to form a three dimensional network, in which molecules are held together by chemical or physical forces.[1-8] As in the case of surfactant, it is well known that above their critical micellar concentration they are able to self-assemble in water to form spherical micellar aggregates, but when the concentration is even higher the micelles give the so-called sphere to rod transition consisting in the growth of the micellar aggregates along one axis.[9-14] These rod-like micelles interact by means of non-covalent interactions (hydrogen bonds, Coulomb interactions, van der Waals forces, …) forming the macroscopic network known as hydrogel. Such medium, which has the appearance and rheology behaviour of solids,[15-19] characterized by high viscosity and low mobility, is made up of hydrophilic water pools surrounded by hydrophobic intertwined wormlike micelles.[1,20,21] In this work, we resorted to a zwitterionic amine N-oxide-surfactant (*p*DoAO) to form a viscous gel in pure water.[22] The morphological characterization of the *p*DoAO hydrogel, carried out by means of Scanning Electron Microscopy, revealed the presence of non-uniformly distributed pores with an average diameter of 10 μm.[23] Rheology measurements were performed on aqueous solutions of *p*DoAO: a typical behaviour of a viscoelastic material was observed, with values of relaxation time and zero-shear viscosity much larger than those observed with other viscoelastic wormlike systems formed by amine-oxide surfactants.[22] Interestingly, *p*DoAO solutions exhibit these properties without any kind of additive. Since the N-oxide surfactant has a dissociation constant of 4.9, its three dimensional network loses compactness at pHs ≤ 4 (as revealed by viscosity measurements and dynamic light scattering studies).[22] This pH sensitivity is useful when the gel is exploited as drug vehicles: it can swallow the desired drugs and carry them through the human body, where it delivers the antibiotics coming across specific pH conditions. For this purpose, the biocompatibility of the surfactant is also of utmost interest and clearly deeply required. Amine-oxide surfactants are extremely appealing over their cationic counterpart due to their low toxicity and easier biodegradability.[22] Moreover, the breaking response of their gel network to an increase in the acidity of the environment is desirable, being the inside of some

cellular compartments characterized by low pHs compared to the physiological pH of the blood plasma.[24-28]

On the other hand, tetracycline drugs are a family of natural and synthetic compounds which have been widely studied since their discovery in the 1940s. Since then, their applications have been spreading from the one as broad-spectrum antibiotics to that as regulators of gene expression.[29-31] Even though some bacteria have developed mechanisms of resistance to these drugs,[29] their diverse applications make them still worth of investigation. Moreover, tetracyclines show a complex acid-base behaviour in aqueous solutions[32-34]. For instance, it has been demonstrated that the differently protonated forms of Tetracycline (TC), Oxytetracycline (OX) and Doxycycline (DX) have utterly different properties with respect to the interaction with both biologically relevant cations[35-38] (whose complexes represent the active species against the bacterium) and surfactant micelles[39,40]. TC, OX and DX have been already investigated in our laboratories in the presence of an analogous cationic quaternary ammonium surfactant p-dodecyloxybenzyltrimethylammonium bromide (pDoTABr), whose micelles proved a smart supramolecular behavior.[39,40] Although no considerable interaction was found between TC and these micelles, the latter are able to swallow the zwitterionic OX and DX at pH 5.0, whereas the mono-anionic OX and DX, prevailing at pH 8.9, interact strongly with the micellar cationic surface. Furthermore, the addition of magnesium cations triggers the release of the drug into the bulk aqueous solution as metal-chelates ready to act against the bacteria. It seems therefore worthy to develop the investigation, including further organized media which can open up new possibilities of smart drug delivery.

Thus, combining the features of the amphoteric amine-oxide surfactant with that of the tetracycline drugs, a prototype of a drug-vehicle system can be attained. The possibility of loading the hydrogel with two molecules belonging to the family of tetracyclines, namely OX and DX, has been investigated by means of spectroscopic techniques and the results are described in this paper. The spectral properties of DX and OX are widely known; they are sensitive to the environment experienced by the molecule. The changes in the absorption, emission and excited-state absorption properties recorded for DX and OX demonstrate the inclusion of the drugs within the hydrophobic domains provided by the hydrogel, which in turn modulates the drug properties.

Experimental Section

Chemicals and Samples

Oxytetracycline dehydrate (OX) and Doxycycline hyclate (DX) (Scheme 1) were used as purchased from Sigma-Aldrich ($\geq$ 98% and $\geq$ 97%, respectively), without any further purification. Ethanol 95% (EtOH), methanol (MeOH) and glycerol (Gly) were from Sigma-Aldrich and used without further purification. The drugs were dissolved in buffered water (pH values of 2.2, 5.0 and 8.9) at concentrations ranging from slightly lower than $1 \cdot 10^{-5}$ M for fluorimetric measurements to ten times greater for all the other experiments. $MgCl_2$ anhydrous salt was furnished by Fluka Solutions and dissolved in the buffers to provide stock metal cation solutions at concentrations nearly 1 M at acidic pHs and $4 \cdot 10^{-2}$ M at basic pHs. Britton buffers were used to achieve the desired pH values by titrating a mixture of acids (H_3BO_3 0.04 M, H_3PO_4 0.04 M and CH_3COOH 0.04 M) with a 0.2 M solution of NaOH. Deionized water was added to the solutions in order to attain the same ionic strength of 5 mM for all of the buffers.

R1 = H; R2 = CH$_3$; R3 = OH; R4 = OH (OX)

R1 = H; R2 = CH3; R3 = H; R4 = OH (DX)
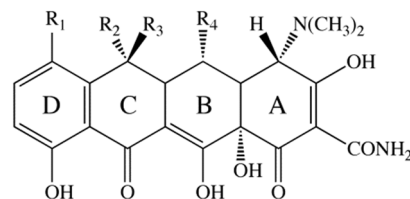
Scheme 1. Molecular structure of the investigated tetracyclines.
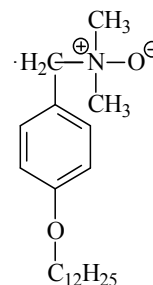
Scheme 2. Molecular structure of the surfactant p-dodecyloxybenzyldimethylamine N-oxide (pDoAO).

The pDoAO zwitterionic surfactant (Scheme 2) was synthesized in our laboratories.[41] pDoAO is able to self-assemble in pure aqueous solutions to form hydrogels at relative low concentration (0.05 M) and thus, it was used at concentration 0.067 M to provide a viscous environment for both the free molecules and their complexes with Mg^{2+}. In order to form a macroscopically homogenous hydrogel matrix, solutions of pDoAO at 0.1 M concentration were prepared. The gel, being thermoreversible, was then heated, up to 80° C, and stirred, to liquefy and take 2 mL of the sample to be put in the cuvette for the analysis. 1 mL of the solutions containing the drug alone or together with Mg^{2+} in proper ratios were then added into the cuvette and homogenized with the hydrogel by means of further heating. The samples were left overnight to rest and cool down to room temperature to be ready for the spectroscopic analysis.

Photophysical Measurements

Steady–state absorption and emission spectra were recorded with a Perkin Elmer Lambda 800 spectrophotometer and a Fluorolog-2 (Spex, F112AI) spectrophotofluorometer, respectively. The latter gives back fluorescence emission spectra taking into account both the monochromator response and the detector sensitivity. Fluorescence quantum yields (experimental error of ca. 7%) were determined from the emission spectra of samples whose absorbance at the excitation wavelength was lower than 0.1, to have a linear relation between the absorbance and the emitted intensity and avoid self-absorption effects. Fluorescein, whose Φ_F has been previously found to be 1 in pDoAO hydrogel at pH 9,[39] was used as a standard to determine the quantum yields of the free drugs and their complexes in this viscous medium.

The fluorescence lifetimes (τ_F) were measured by a spectrofluorometer based on the single photon counting technique, equipped for the systems under investigation with a LED source centred at 370 nm using an interference filter centred at 366 nm in

the excitation line and a long-pass filter in emission at 488 nm. The resolution time of the experimental set-up is 0.5 ns when a LED source is used.[42] All the data acquired were analyzed by IBH Data Analysis software; the program allows to deconvolve the decay profile of the source from the sample decay and provides the fitting of the data, whose goodness is evaluated by means of residuals distribution and the χ^2 value.

The experimental setup for ultrafast spectroscopic and kinetic measurements has been widely described elsewhere.[43,44] Briefly, the 400 nm excitation pulses of ca. 40 fs were generated by an amplified Ti:Sapphire laser system (Spectra Physics, Mountain View, CA). The transient absorption set up (Helios, Ultrafast Systems, Sarasota, FL) is characterized by temporal resolution of ca. 150 fs and spectral resolution of 1.5 nm. Probe pulses for optical measurements were produced in the 475-750 nm range by passing a small portion of 800 nm light through an optical delay line (with a time window of 3200 ps) and focusing it into a 2 mm thick Ti:Sapphire window to generate a white-light continuum. The chirp inside the sample cell was determined by measuring the laser-induced Kerr signal of the solvent. The femtosecond time-resolved fluorescence spectroscopy employs the up-conversion technique (Halcyone, Ultrafast Systems).[45] The femtosecond laser pulses (the 800 nm and its second harmonic 400 nm) are generated by the same amplified mode-locked Ti-sapphire laser system used in the transient absorption experiments. The second harmonic, after passing through a half wave plate, excites the sample. The remaining fundamental laser beam passes through an optical delay line with a time window of 3200 ps and is then used as the "optical gate". The fluorescence of the sample is collected and focused onto a BBO crystal (1.5 mm thickness) together with the delayed fundamental laser beam. The up-converted fluorescence beam is focused into the entrance of a monochromator by a lens, and it is detected by a photomultiplier connected to a photon counter having an exposure time equal to 2 s at each delay point. The resolution of the time-resolved fluorescence equipment is about 250 fs, whereas the spectral resolution is 5 nm. All the measurements were carried out under magic angle, in a 2 mm cell and with an absorbance ranging from 0.3 to 1.0 at 400 nm. The samples were kept in constant movement by a translational sample holder (Ultrafast Systems) controlled by two NSC200 controllers (Newport, Irvine, CA), for horizontal and vertical displacement respectively, to prevent local photodegradation of the non-diffusing medium. Transient absorption data were analyzed using the Surface Xplorer PRO (Ultrafast Systems) and the Glotaran software.[46] The first allows one to perform Singular Value Deconvolution of the 3D surface into principal components (spectra and kinetics) followed by Global Analysis (giving lifetimes with an error of ≈10% and Decay Associated Spectra, DAS, of the detected transients).[47] Glotaran was used to perform the Target Analysis to carry out the global fit of the acquired data and provided the Species Associated Spectra (SAS).[47]

Kinetic traces at chosen wavelengths were also analyzed by means of the Maximum Entropy Method (MEM) by means of the MEMEXP Software available online.[48,49] In the Maximum Entropy Method the experimental decay A(t) is fitted by the following function:

$$A(t) = D_0 \int\limits_{-\infty}^{+\infty} d\log\tau [g(\log\tau) - h(\log\tau)] \times$$
$$\int\limits_{-t_0}^{\min(t,t_f)} dt' R(t') e^{-(t_i - t')/\tau} + \sum_{k=0}^{3}(b_k - c_k) \qquad (1)$$

where $g(\log\tau)$ and $h(\log\tau)$ are the lifetime distributions that correspond to decay and rise kinetics, respectively, D_0 is a normalization constant, and the polynomial term accounts for the baseline. The instrument response function R(t) is peaked at zero time and is appreciable only in the interval [-t_0, t_f]. The fit procedure entails the maximization of the function Q defined in equation (2):

$$Q = S - \lambda C - \alpha I \qquad (2)$$

In equation (2), S is entropy defined as

$$S(\vec{f}, \vec{F}) = \sum_{j=1}^{M}[f_j - F_j - f_j \ln(f_j / F_j)] \qquad (3)$$

where f is the image that includes both the g and the h lifetime distributions, whereas F is the MEM prior distribution used to incorporate prior knowledge into the solution. C is a measure of the quality of the fit F to the data. When we analyzed the kinetic traces of femtosecond transient absorption with normally distributed noise, C was the χ^2. For Poisson-distributed data like those collected by the single photon counting technique, C was the Poisson deviance. I is a normalization factor; λ and α are Lagrange multipliers. The method, which is based on the simultaneous maximization of the entropy (S) and minimization of C (2), gives back the distribution of lifetimes, as well as the number of transients (family of distributions around an average time) needed to describe the spectroscopic kinetics. These distributions describe the probability of having different lifetimes. The widths of the distributions are sensitive to the heterogeneous microenvironment a molecule can experience in the sample.[50,51]

Results and Discussion

Steady-state Absorption and Fluorescence Spectra

It is known that DX and OX undergo three consecutive deprotonations in water at pKa values of 3.40, 7.70, 9.30,[52] and 3.27, 7.32, 9.11,[53] respectively. Therefore, four differently protonated forms (cationic, zwitterionic, monoanionic and bianionic) can be retrieved at equilibrium in water for both molecules. DX and OX have been previously studied at four distinct buffered pH values (i.e. roughly 2, 5, 9, 11) in order to investigate the photophysical properties of each protonated form.[38,40] Moreover, it has been already proved by means of fluorimetric titrations and ultrafast time resolved techniques that no acid-base re-equilibration takes place in the excited state of tetracyclines.[40]

The present study has been performed at pH values of 2.2, 5.0 and 8.9. At pH 2.2, the drugs are in their cationic forms while the hydrogel loses its three-dimensional intertwined structure due to its complete protonation (the pKa of *p*DoAO is 4.9). At pH 5.0 and 8.9 the drugs are in their zwitterionic and mono-anionic forms, respectively.

The visible absorption spectrum of the tetracycline drugs in aqueous solution is characterized by a band centred in the interval 345-375 nm whose maximum shifts depending on the protonation state of the molecule; the fluorescence emission spectrum shows a broad band whose maximum ranges from 600 nm for the protonated drug to 520 nm for the bi-anion form, whose fluorescence quantum yield is one order of magnitude higher than that of the protonated form (~10^{-3} instead of ~10^{-4}).[34,38]

Table 1. Absorption and fluorescence properties of DX, OX and their complexes with Mg^{2+} at different pHs in *p*DoAO hydrogel ([*p*DoAO] = 0.067 M).

pH	system	λ_{abs}(nm)		λ_{em} (nm)		Stokes shift (cm^{-1})		Φ_F	
		solution	gel	solution	gel	solution	gel	solution	Gel
2.2[a]	DX	345	355	605	540	12500	9700	0.00038	0.012
	OX	355	350	585	465	11700	7100	0.00063	0.035
5.0	DX	345	365	600	515	12300	8000	0.00049	0.010
	DX-Mg^{2+}	370	375	545[b]	520	8700	7400	0.0058[b]	0.038
	OX	355	360	585	465	11500	6300	0.00089	0.056
	OX-Mg^{2+}	370	371	530[b]	525	8200	7900	0.018[b]	0.029
8.9	DX	365	371	540	495	8900	6800	0.0011	0.013
	DX-Mg^{2+}	370	377	535[b]	505	8300	6700	0.011[b]	0.11
	OX	365	364	530	460	8200	5700	0.0021	0.079
	OX-Mg^{2+}	370	374	530[b]	520	7800	7500	0.016[b]	0.069

[a]Data for the complexes with Mg^{2+} at pH 2.2 could not be stored because of the precipitation of the surfactant, promoted by a salting out phenomenon. [b]Emission maximum and fluorescence yield obtained after the last addition of Mg^{2+} in the cuvette.

The absorption and emission properties of DX and OX and their complexes with Mg^{2+} in *p*DoAO hydrogel are summarized in Table 1, where the same properties in water are shown for comparison. It is clear that when the drugs are in the gel the Stokes shift reduces, whereas the fluorescence quantum yield increases with respect to the values determined in water. This evidence suggests the inclusion of the drugs in the hydrophobic micro-environment of the gel. In particular, for free DX, the effect of the viscous environment is clearly to red shift the absorption spectrum as well as to blue shift the emission band (Fig. 1), resulting in a significant reduction of the Stokes shift for the free drug under all the pH conditions investigated. On the other hand, OX shows an even more significant hypsochromic shift of the fluorescence band (centred at 460–465 nm in the organized media), but its absorption spectrum stays nearly unchanged at basic pHs and undergoes a minor red shift at acidic pHs. The absorption band at basic pHs, however, looks broader than the same in pure water, being sensitive to the micro-heterogeneous environment provided by the hydrogel (Fig. 1, bottom right-hand panel). From this evidence the inclusion of the molecules in the hydrophobic domain of the hydrogel is confidently inferred.[39]

As far as Mg^{2+} complexes are concerned, we know from our previous works that the complexation in aqueous solution is responsible for an enhancement of the fluorescence quantum yield and a reduction of the Stokes shift for both molecules.[38] The reason of this behaviour can be attributed to the formation of a six-membered chelate ring structure with the metal ions, with the consequent lack of excited state vibrational relaxation through hydrogen bonding with the solvent. When the Mg^{2+} complexes are studied in the hydrogel medium, a further reduction of the Stokes shift (due to a little bathochromic shift of the absorption and a distinct hypsochromic shift of the emission band) can still be revealed for both molecules with respect to the analogous data retrieved in aqueous solution. The Stokes shift reduction induced by the gel is smaller for the complexes rather than for the free substrates. This evidence suggests the free molecules are more easily enclosed inside the hydrophobic domains than the metal chelates, because the latter are electrically charged and thus allied to the polar and dielectric aqueous pools, as clearly demonstrated by time resolved investigation (see below).
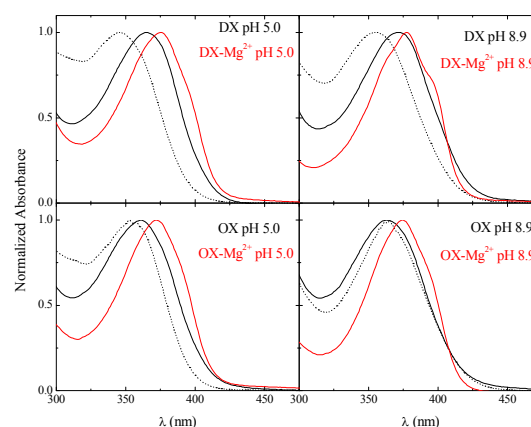
Figure 1. Absorption spectra of DX (upper panel) and OX (lower panel) (~ 1 x 10^{-5} M) in water (dashed lines) and in gel ([*p*DoAO] = 0.067 M) at pH 5.0 (left) and at pH 8.9 (right) alone (black lines) and in the presence of Mg^{2+} in concentration 0.08 M at pH 5.0 and 0.003 M at pH 8.9 (red lines).
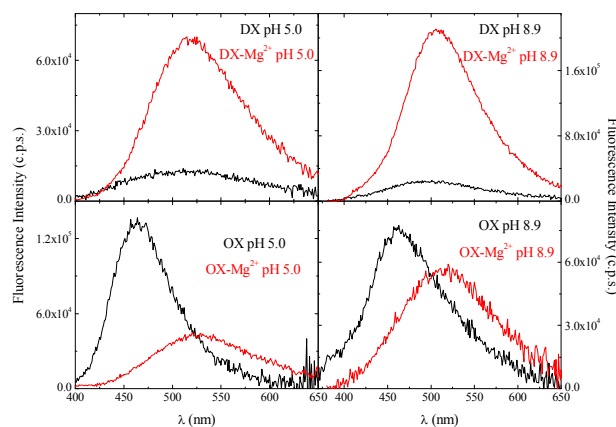
Figure 2. Emission spectra of DX (upper panel) and OX (lower panel) (~ 1 x 10^{-5} M) in gel ([*p*DoAO] = 0.067 M) at pH 5.0 (left) and at pH 8.9 (right) alone (black lines) and in the presence of Mg^{2+} in concentration 0.08 M at pH 5.0 and 0.003 M at pH 8.9 (red lines).

The changes revealed in the fluorescence quantum yield help to understand the effectiveness of the substrate permeation within the swollen matrices. In fact, both free drugs and their Mg^{2+}-complexes show an enhanced fluorescence efficiency with respect to what was previously observed in solution, supposedly due to the confinement of some molecules in a less polar and more viscous environment, which is able to foster the emission deactivation pathway over the non-radiative ones.[54] Free DX undergoes a fluorescence enhancement with respect to its emission in water of 10-30 times at different pHs; a similar trend is revealed for free OX, but this time the increase is over 50 times at acidic pHs and nearly 40 times at pH 8.9. Comparing the two molecules, one can deduce a much greater affinity of OX for the gel: its fluorescence properties in this hydrophobic and viscoelastic medium are indeed greatly altered.

In order to associate the fluorescence enhancement to the physical properties of the organized medium, emission quantum yields of DX and OX in some solvents characterized by different polarities and viscosities have been evaluated. The results obtained in ethanol, methanol and a methanol/glycerol mixture compared with those obtained in water are shown in Table 2. The fluorescence efficiency for both drugs decreases upon increasing the solvent polarity (on going from ethanol to water) and increases significantly upon increasing the solvent viscosity (on going from methanol to a methanol/glycerol mixture). The changes in the fluorescence quantum yields induced by the hydrophobic and viscoelastic gel are therefore likely due to a combined polarity and viscosity effect for both molecules.

Table 2. Fluorescence quantum yields of DX and OX in solvents of different polarity and viscosity.

Compound	Solvent	ϕ_F
DX	EtOH	0.0042
	MeOH	0.0035
	MeOH/Gly 50/50	0.012
	Water	0.0011
OX	EtOH	0.0094
	MeOH	0.0048
	MeOH/Gly 50/50	0.015
	Water	0.0021

The two molecules show a diametrically opposite behaviour when their complexes are considered: the fluorescence of DX-Mg^{2+} chelate increases by nearly one order of magnitude with respect to the same system in water; on the other hand OX-Mg^{2+} chelate emission increases only by a factor of 2÷4. The complexes permeation within the micellar gel is therefore greater in case of DX than in that of OX.

All these spectroscopic variations confirm a greater affinity of free OX for the hydrophobic domains with respect to DX, but also a more efficient inclusion of DX-Mg^{2+} complexes rather than OX-Mg^{2+} chelates, which is quite impressive taking into account the extremely similar structures of the two molecules. In fact, both free drugs are effectively loaded into the gel phase (as the time resolved spectroscopic study proved, see below); the greater alteration of the properties of OX induced by the inclusion into the matrix must be therefore due to a specific interaction of free OX with the pDoAO surfactant. This interaction supposedly involves a hydrogen bond between the additional –OH group (in the R_3 position) characterizing OX with respect to DX and the negatively charged oxygen of the amine-oxide surfactant. When the magnesium complexed DX and OX are considered, we are dealing with a much more

complicated system for which a clear rationalization is very difficult. However, we can speculate that the interaction with magnesium interferes with the specific interaction of OX and the surfactant leading to a more efficient inclusion in the gel phase of the chelates of the less hydrophilic DX.

Time-resolved Fluorescence Properties

The fluorescence kinetics describing the deactivation of the excited state of DX and OX in pDoAO hydrogel was successfully measured by means of the ns-resolved TC-SPC technique. In fact, because of the small quantum yields and the resulting fast deactivation times (tens of ps for the free molecules and a few hundreds of picoseconds for the metal chelates), this kind of measurement is not feasible for tetracyclines in water, but it becomes a valuable investigation tool in organized media, that usually slow down the deactivation of the excited states.[55]

The results obtained by fitting the kinetic traces with exponential functions characterized by the least-squares method are listed in Table 3. Two components are always needed in order to well reproduce the deactivation profile: one is characterized by a time constant close to the time resolution of the instrumentation (~0.5 ns), whereas the other component is much longer (ranging from 1.5 ns in the case of some complexes with magnesium to 3.4 ns in the case of free OX).

Once again, the two molecules show a different behaviour both as free molecules and as metal chelates. The relative amplitudes of the two components are indeed revealing: the emission of free DX exhibits roughly the same contribution arising from the two components, whereas free OX deactivation is dominated by the longer component. These findings are in agreement with the steady state measurements, which revealed greater spectral changes induced by the gel in the case of free OX rather than in the case of free DX. However, the appearance of decay times on the sub-nanosecond and nanosecond time scale for the free drugs studied in hydrogel, much longer than the one detected in pure aqueous solution (around 20 ps), is undoubtedly due to molecules confined in the hydrophobic domains of the gel. The two emitting components are therefore likely due to two different tautomeric forms of the drugs, both embedded in the gel phase.

On the other hand, when one is dealing with the Mg^{2+}-complexes, the prevailing component is the longer one in the case of DX, vice versa for OX: after all, even the steady-state fluorescence properties of DX complexes were more greatly altered by the gel than those of OX complexes. In order to try an assignment of these two components, analogous measurements were carried out on the same complexes in water and in the presence of the surfactant at high temperature before the gelification had taken place. The kinetics acquired with the TC-SPC technique were analyzed by means of the MEM method, whose results are shown in Figure 3. Comparing the three profiles one can deduce a clear broadening of the time distributions on going from the homogenous aqueous solution to the more complex gel medium: in pure water all the molecules experience the same environment and their deactivation time is well-defined (black trace); as long as the solution is still fluid (red trace) the time distribution becomes a little broader, though it is still centred at a time close to the one detected in water (~0.5 ns). When the gel network is formed and a major micro-heterogeneity is attained in the sample, the distribution becomes much broader and a tail in the case of OX-Mg^{2+} (Fig. 3 upper graph) and a proper band in the case of DX-Mg^{2+} chelates (Fig. 3 lower graph) appear in the profile. As the

simple exponential fitting pointed out, a second time is needed to well reproduce the decay of the fluorescence in the *p*DoAO gel and the MEM analysis revealed its contribution at times longer than 1 ns, accordingly. Such long-living component, arising only after the gelification occurred, must be related to those Mg^{2+}-complexed molecules able to permeate the gel network and be swallowed by the hydrophobic matrix. The greater weight of the longer living component of DX-Mg^{2+} complexes pointed out by the exponential fitting and confirmed by the MEM analysis is an indicator of their more favourable inclusion in the gel phase.

Table 3. Fluorescence lifetimes (obtained by using the ns-resolved TC-SPC technique) and relative amplitudes of DX, OX and their complexes with Mg^{2+} in *p*DoAO hydrogel ([*p*DoAO] = 0.067 M) at different pHs.

| System	pH								assignment
	2.2		5.0		deionized-H_2O		8.9		
	τ (ns)	relative amplitude	τ (ns)	relative amplitude	τ (ns)	relative amplitude	τ (ns)	relative amplitude	
DX	<0.5	57.1%	<0.5	56.4%	<0.5	53.8%	<0.5	49.9%	S_1 (DX_1) gel
	3.1	42.9%	2.9	43.6%	2.4	46.2%	2.4	50.1%	S_1 (DX_2) gel
OX	<0.5	19.4%	<0.5	12.0%	<0.5	18.4%	<0.5	23.2%	S_1 (OX_1) gel
	3.4	80.6%	3.3	88.0%	3.1	81.6%	2.9	76.8%	S_1 (OX_2) gel
DX-Mg^{2+}	-	-	<0.5	28.4%	<0.5	18.1%	<0.5	23.3%	S_1 (DX-Mg^{2+}) water
	-	-	1.8	71.6%	1.7	81.9%	1.7	76.7%	S_1 (DX-Mg^{2+}) gel
OX-Mg^{2+}	-	-	<0.5	78.8%	<0.5	67.1%	<0.5	69.6%	S_1 (OX-Mg^{2+}) water
	-	-	1.7	21.2%	1.6	32.9%	1.6	30.4%	S_1 (OX-Mg^{2+}) gel
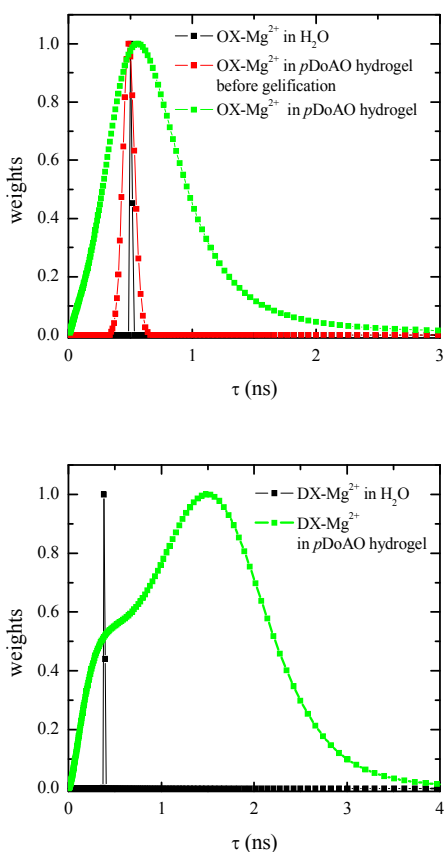
Figure 3. Results of the MEM analysis of the fluorescence decay kinetics acquired by means of the TC-SPC technique for OX-Mg^{2+} (upper graph) and DX-Mg^{2+} (lower graph) in solution (black trace) and in *p*DoAO before and after the gelification, (red and green traces, respectively).

The kinetic behaviour of the two molecules was also investigated at pH 2.2, where the hydrogel loses its compactness and it is thus likely to release the drugs into the bulk aqueous solution to a certain extent. In order to reveal those molecules expected to be dissolved in water, the ns-resolved TC-SPC technique does not have the needed time resolution and a femtosecond resolved equipment is therefore required. Fluorescence up-conversion measurements were performed on DX and OX at pH 2.2. Data were collected at wavelengths chosen in order to match the emission maxima of the steady-state fluorescence spectra in gel and in solution (Figure 4 and Table 4). The kinetics of OX is well reproduced by means of five components whose time constants are τ_1=0.40 ps (S), τ_2=2.0 ps (S'), τ_3=26 ps (M), τ_4=280 ps (L) and τ_5=3400ps (L'), the last one fixed in agreement with the TC-SPC measurements. The two longer-lived transients (L and L') are assigned to the two species commonly observed in the gel phase; the shortest components (S and S') are likely due to solvent reorganization and/or vibrational cooling phenomena, and the M component is supposedly associated with the anticipated molecules in the aqueous phase. As for OX, the measurements for DX were performed at about 500 and 600 nm, in correspondence to the two maxima of DX in gel matrix and water, respectively. The kinetics are well-fitted by exponential functions with five components. The two shortest components with τ_1=0.41 ps and τ_2=1.9 ps as lifetimes, are due to solvent re-equilibration and vibrational relaxation too. The longest components with time constants of 440 and 3100 ps, are relative to the emitting states. Finally, the fifth component with a lifetime of 53 ps is much longer than the S_1 state of the DX drug previously observed in aqueous solution (τ~14 ps).[40] The 53 ps lifetime is also shorter than the times detected for molecules in the hydrogel phase. Spectral information associated to kinetics data, acquired by femtosecond transient absorption measurements, become therefore crucial for a straightforward assignment of this unexpected component (see next paragraph).
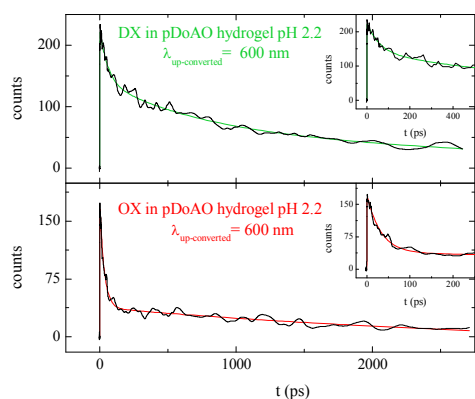
Figure 4. Fluorescence decay kinetics recorded by the up-conversion technique for DX (upper panel) and OX (lower panel) in gel at pH 2.2 (black traces) and their fitting (green and red traces, respectively). Insets: zoom in on the first part of the kinetics traces.

Table 4. Fluorescence lifetimes (obtained by using the fluorescence up-conversion technique) of DX and OX in gel at pH 2.2.

pH	system	τ(ps)	assignment
2.2	DX	0.41	Solv.$_i$
		1.9	Solv.$_d$ /VC
		53	S_1(DX) non-gel
		440	S_1(DX$_1$) gel
		3100	S_1(DX$_2$) gel
	OX	0.40	Solv.$_i$
		2.0	Solv.$_d$ /VC
		26	S_1(OX) non-gel
		280	S_1(OX$_1$) gel
		3400	S_1(OX$_2$) gel

Femtosecond Transient Absorption

To get a deeper insight on the relaxation dynamics of DX and OX as both free molecules and Mg^{2+}-chelates, in gel at different pHs, we performed femtosecond transient absorption experiments.

Except for pH 2.2 which will be discussed aside because of its peculiarity, the transient spectrum evolution, acquired over a time window of about 3200 ps after excitation of the sample at 400 nm, shows two main contributions: a broad region of negative signal centred around 550–575 nm spectral range (depending on the system) that is stimulated emission, and a transient absorption signal (not always clearly detectable) above 650 nm (Fig.s 5 and 6, panels B). The 3D-data sets were analyzed by the Global Analysis and Target Analysis fitting procedures, while single wavelength decays by the Maximum Entropy Method (MEM), in order to be confident of the number of transients deduced and their time constants.

The results of the Target Analysis are listed in Table 5 and shown in Figures 5 and 6, panels C, in the case of free DX at pH 5.0 and 8.9, respectively.

As far as free molecules are concerned, under both pH conditions the data are described by five transients. The rest absorption is attributed to the triplet state of the molecule formed by intersystem crossing.[34] The two shortest components

(hundreds of femtoseconds and few picoseconds, respectively) are similar to the same components detected in water (which is still largely present in the gel) and assigned to solvent equilibration phenomena accordingly.[56] Yet, the one with a time constant of few picoseconds, that is longer for DX rather than OX and it slows down at pH 8.9, must account for some contribution of the vibrational cooling; in fact, the longer the time constant, the more red-shifted the spectrum respect to excitation wavelength of 400 nm.

The longest transients are characterized by a broad negative band of stimulated emission and decay times close to those detected by TC-SPC. Therefore, they are attributed to the same emitting species.
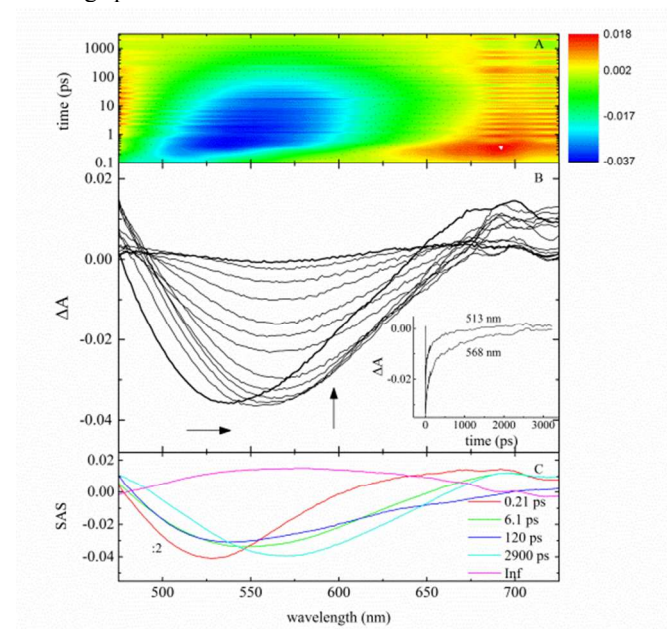

Figure 5. Pump-probe absorption spectroscopy of DX in gel at pH 5.0 (λ_{exc}= 400 nm; [pDoAO] = 0.067 M): A) contour plot of the experimental data; B) time resolved absorption spectra recorded at increasing delays after the laser pulse (the very first spectra and the last one are represented by ticker lines). Insets: decay kinetics recorded at meaningful wavelengths and C) amplitudes of the SAS obtained by Target Analysis.

If we look at the SAS (Species Associated Spectra) at the two pHs, it emerges that there are no differences. Moreover, the positions of the bands at pH 5.0, compared to the same results in pure aqueous solutions, are significantly blue-shifted with respect to that of the zwitterion (λ = 675–690 nm), getting closer to those of the two tautomers of the monoanion form of tetracyclines. It is therefore likely that at pH 5.0 the zwitterionic drug experiences a gel induced deprotonation, which promotes the presence of the monoanion even under acidic pH conditions. The possibility of an apparent change of the acidity of the whole sample was ruled out by checking the pH of the bulk gel medium after the gelification had taken place. Nonetheless, a careful analysis of the transient spectral shapes of both DX and OX at pH 5.0 reveals a shoulder at longer wavelengths (λ > 650nm) in the region of the stimulated emission previously detected for the zwitterionic form of the tetracycline molecules (Figure 5, panel C). The existence of a certain amount of molecules in the zwitterionic form has to be invoked, thus explaining the persistent slight changes of the steady-state spectral properties still found between pH 5.0 and 8.9. The two transients, however, can be nothing else but the

two tautomers of the monoanion already detected in pure water solution and in the presence of cationic *p*DoTABr micelles at pH 8.9, although their time constants are increased by the viscous environment provided by the gel. Once again, as in the case of the micellar solution, the organized medium shifts the tautomeric equilibrium towards the longer-lived species, as it is also confirmed by the MEM analysis performed on the data of DX at pH 8.9, shown in Figure 7 in comparison to the same results obtained in aqueous solution.

Independently of the molecule, the abundance of the longer-lived tautomer is larger than in water, but in spite of the relative amplitudes found in the TC-SPC experiments, there is no significant variations between DX and OX: the greater contribution of this ns-living transient and the greater effect on the emission properties in the case of OX, may be due to the intrinsic higher fluorescence quantum yields of this tautomer, whose decay time is also longer (~ 3 ns).

Table 5. Spectral and kinetic properties of the excited states of DX, OX and their complexes (1:1 and 1:2) with Mg^{2+} in *p*DoAO hydrogel at different pHs (λ_{exc}=400 nm) obtained by Target Analysis.

| pH	system	τ(ps)	λ(nm)	assignment
5.0	DX	0.21	525(−), 675(+)	Solv.$_i$
		6.1	545(−), 695(+)	Solv.$_d$ /VC
		120	540(−)	S_1 (DX1) gel
		2900	570(−), 690(+)	S_1 (DX2) gel
		Inf	575(+)	T_1
	DX-Mg^{2+}	0.19	525(−), 625(+)	Solv.
		13	530(−)	S_1 (1:1A) water
		260	555(−)	S_1 (1:2A,BCD) water
		1800	555(−)	S_1 (1:2A,BCD) gel
		Inf	595(+)	T_1
	OX	<0.1	540(−), 675(+)	Solv.$_i$
		2.8	545(−), 680(+)	Solv.$_d$ /VC
		79	555(−)	S_1 (OX1) gel
		3000	575(−), 690(+)	S_1 (OX2) gel
		Inf	580(+)	T_1
	OX-Mg^{2+}	0.17	520(−), >575(+)	Solv.
		19	530(−)	S_1 (1:1A) water
		310	555(−)	S_1 (1:2A,BCD) water
		1700	560(−)	S_1 (1:2A,BCD) gel
		Inf	605(+)	T_1
8.9	DX	0.23	525(−), 680(+)	Solv.$_i$
		7.4	540(−), 700(+)	Solv.$_d$ /VC
		110	535(−)	S_1 (DX1) gel
		2400	565(−), 700(+)	S_1 (DX2) gel
		Inf	580(+)	T_1
	DX-Mg^{2+}	0.20	510(−), 630(+)	Solv.
		100	540(−), 710(+)	S_1 (1:1BCD/1:2BCD,BCD) water
		1700	550(−), 700(+)	S_1 (1:1BCD/1:2BCD,BCD) gel
		Inf	590(+)	T_1
	OX	0.50	535(−), 680(+)	Solv.$_i$
		4.0	555(−), 700(+)	Solv.$_d$ /VC
		110	550(−),	S_1 (OX1) gel
		2900	570(−), 690(+)	S_1 (OX2) gel
		Inf	580(+)	T_1
	OX-Mg^{2+}	0.17	505(−), 600(+)	Solv.
		12	540(−)	S_1 (1:1A) water
		200	550(−)	S_1 (1:2A,BCD) water
		1600	560(−)	S_1 (1:2A,BCD) gel
		Inf	560(+)	T_1
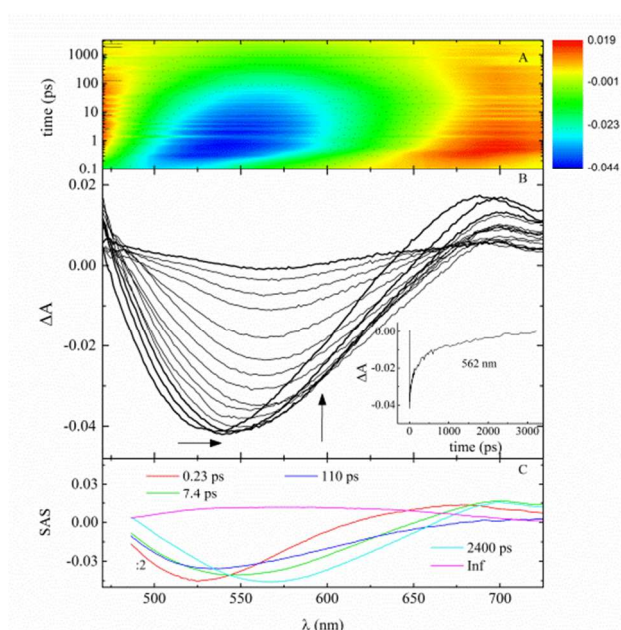
Figure 6. Pump-probe absorption spectroscopy of DX in gel at pH 8.9 (λ_{exc}= 400 nm; [pDoAO] = 0.067 M): A) contour plot of the experimental data; B) time resolved absorption spectra recorded at increasing delays after the laser pulse (the very first spectra and the last one are represented by ticker lines). Insets: decay kinetics recorded at meaningful wavelengths and C) amplitudes of the SAS obtained by Target Analysis.
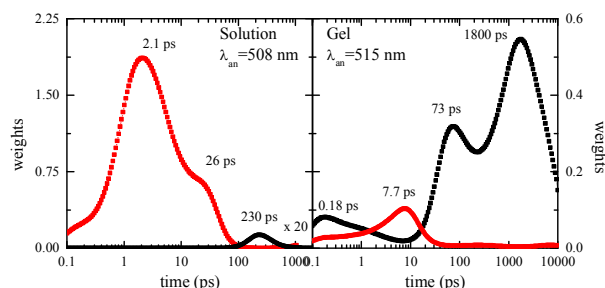

Figure 7. Results of the MEM analysis of the femtosecond transient absorption kinetics at 508 and 515 nm for DX at pH 8.9 in aqueous solution and in pDoAO hydrogel, respectively. The red and black distributions represent growth and decay contributions, respectively.

Measurements at severely acidic pH were performed on both molecules. The data are shown in Figure 8 for DX and summarized in Table 6, where the same data collected in pure aqueous solution at the same pH value of 2.2 are listed for comparison. The spectral evolution is noticeably different from that revealed at the other pHs and characterized by the formation of a broad negative signal of stimulated emission centred at about 600 nm, rising during the first picoseconds after the excitation laser pulse with a shoulder at longer wavelength (Figure 8, inset panel B). The latter shows a rather fast decay, while the minimum of stimulated emission shifts towards the hypsochromic part of the spectrum, being centred at about 570 nm by the end of the temporal scan of 3200 ps (Figure 8 panel B).

The lifetimes retrieved by means of the Global Analysis and those of the Target Analysis are in fair agreement with the up-conversion results (Figure 4), but, giving out the spectral shapes of the diverse transients in addition to their time constants, they

are extremely helpful for the interpretation of the data. The two longer lived transients, with time constants of hundreds and thousands of ps, are described by negative bands centred at about 600 and 570 nm, respectively, and again assigned to the two tautomeric forms of the deprotonated drug trapped in between the persistent gel network. The short component is typical of a sub-picosecond solvent reorganization. The transient of tens of picoseconds, missing at higher pH values, has a spectral shape typical of the zwitterionic or cationic prototropic forms of the tetracycline drugs in solution, with stimulated emission characterized by a minimum at about 700 nm and a shoulder around 600 nm, and transient absorption at shorter wavelengths. Nonetheless, its time constant is 20 ps for OX and approximately 60 ps for DX. The first is fairly close to the time retrieved for cationic OX in solution and thus assigned to the S_1 state of those molecules released in water, but the time constant of DX does not match its counterpart in aqueous solution, as the data of fluorescence up-conversion have already pointed out. Its lifetime is lengthened with respect to the pure aqueous medium, but its spectral shape is not affected: this evidence recalls the behaviour assumed by DX in the presence of the cationic micelles of the analogous ammonium surfactant pDoTABr.[40] In fact, pDoAO is protonated at pH 2.2 and its micelles, though less likely to form a firm hydrogel, are still present in the sample. DX, which had already proven its efficient inclusion in the cationic pDoTABr micelles at acidic pHs, is probably swallowed by the cationic pDoAOH micelles as well, with the resulting lengthening of the S_1 lifetime with respect to the solution.
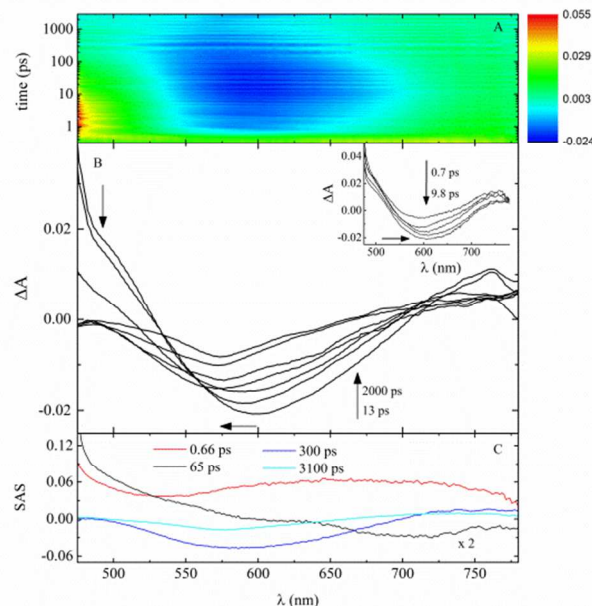

Figure 8. Pump-probe absorption spectroscopy of DX in pDoAO at pH 2.2 (λ_{exc}= 400 nm; [pDoAO] = 0.067 M): A) contour plot of the experimental data; B) time resolved absorption spectra recorded at increasing delays after the laser pulse. Insets: spectra recorded during the first 10 ps after the laser pulse and C) amplitudes of the SAS obtained by Target Analysis.

The greater affinity of OX for the organized medium is indeed lost when the surfactant gets protonated: in this case a preferential inclusion of DX in the micelles resulting from the disruption of the viscoelastic gel is observed. In order to corroborate this hypothesis, time-resolved fluorescence measurements were carried out under the same acidic

conditions in the presence of cationic *p*DoAOH surfactant with its concentration above the c.m.c. but far below the gelification limit: in the case of OX its inclusion within the micellar aggregate is ruled out by the detection of the typical time of the

tetracycline drugs in water (~20 ps), whereas in the case of DX the time constant of about 50 ps supposedly implies its permeation inside the micelles.

Table 6. Spectral and kinetic properties of the excited states of DX and OX in aqueous solution and in *p*DoAO at pH 2.2 (λ_{exc}=400 nm; [pDoAO] = 0.067 M) obtained by Target Analysis.

pH	system	solution		Gel		assignment
		λ (nm)	τ(ps)	λ (nm)	τ(ps)	
2.2	DX	<665(+), 740(-)	0.30	660(+)	0.67	Solv.
		<585(+), 685(−)	13			S_1(DX) water
				<600(+), 700(−)	65	S_1(DX) micelle
		-		580(−), 750(+)	300	S_1(DX$_1$) gel
		-		575(-)	3100	S_1(DX$_2$) gel
	OX	670(+)	0.36	500(+)	0.72	Solv.
		<585(+), 680(−)	18	650(−)	20	S_1(OX) water
				600(−)	500	S_1(OX$_1$) gel
				590(−)	3400	S_1(OX$_2$) gel
				700(+)	Inf	T_1(OX)

As far as the complexes with Mg^{2+} studied at pH 5.0 and 8.9 are concerned (Table 5), the two longest transients, except for the rest absorption, must be the same emitting species revealed by means of the ns-resolved TC-SPC technique. Their lifetimes are hundreds of picoseconds and some nanoseconds, respectively. According to analogous measurements carried out on the parent molecule TC,[39] these two species should be assigned to the complex with magnesium in stoichiometry 1:2 drug:metal ion, which is largely predominant in the sample given the concentrations used in the various experiments.[38] Their spectral shapes are rather similar, and the significant difference in the lifetime must arise from the different environment experienced and therefore reflected by the two transients: the water pools and the hydrophobic domains, respectively. Comparing DX and OX, one can deduce a greater contribution for the longer-lived transient, and thus for those molecules in the gel phase, in the case of DX: the lifetime of the metal chelates in the hydrophobic domains (1600–1800 ps) is almost independent of the molecule structure, but their relative amplitude in the case of the calculated SAS as well as in the case of the TC-SPC measurements is more significant for DX rather than for OX, in agreement with the larger fluorescence quantum yields evaluated for DX-Mg^{2+} rather than for OX-Mg^{2+} complexes.

All of this evidence pointed out a peculiar behaviour of the two molecules and their complexes. Both free drugs are efficiently swallowed by the hydrophobic gel network, as revealed by the appearance of two long-lived transients missing in pure water. On the other hand, the protonation of the surfactant or the complexation of the drugs with magnesium are responsible for a significant release in the aqueous domains, especially in the case of OX. Moreover, as far as metal chelates are concerned, their distribution between the water and gel phase can be elucidated by the relative amplitudes of the two longer transients revealed by means of femtosecond transient absorption measurements and supported by time-resolved fluorescence data.

Conclusions

The loading of a zwitterionic amine oxide (*p*DoAO) hydrogel matrix with OX and DX tetracycline drugs was found to be extremely

efficient under mildly acidic and basic pH conditions. The spectral and emission properties of DX and OX, sensitive to the polarity and viscosity of the medium experienced, are altered by the gel in the same way as it was previously found for the analogous cationic surfactant (*p*DoTABr) micelles,[40] in agreement with the confinement of the molecules in a strongly restrained and hydrophobic environment of the gel.

Differently from *p*DoTABr micelles, for which DX showed a greater affinity, *p*DoAO hydrogel was found to better swallow the OX drug. Moreover and unlike cationic micelles, whose capability of absorbing the drug was related to the prototropic form of the latter, the investigated hydrogel proved to be able to modulate the acid-base behaviour of the drugs: thanks to femtosecond transient absorption results, which appear to be quite alike at pH 5.0 and pH 8.9, a gel induced deprotonation of the zwitterionic tetracyclines was then deduced.

As far as pH 2.2 is concerned, it is well-known that severely acidic pHs are responsible for the protonation of the zwitterionic amphoteric surfactant forming the hydrogel, thus affecting the stability of the three dimensional gel network.[23] This phenomenon can be exploited for the controlled release of the drugs under acidic pH conditions. Such property, if combined with a pH oscillator, may be exploited to produce pulsating drug delivery devices[57] and artificial glands rhythmically realising hormones.[58] In addition to a loss of compactness, visible to the naked-eye, the release of DX and OX into the bulk aqueous solutions was detected again thanks to time resolved techniques. In particular, femtosecond transient absorption and fluorescence up-conversion reveal the presence of a transient assignable to some molecules dissolved in water, in the case of OX, or inside the resultant cationic micellar aggregate, in the case of DX.

On the other hand, the chelation with Mg^{2+} cations causes a clear distribution of the complexes between the two phases: the hydrophobic micellar network and the basically aqueous pools. This time, the Maximum Entropy Method (MEM) analysis was the added value to the interpretation of the data: thanks to this powerful means of analysis, it was possible to distinguish two families of times, assigned to molecules in the two utterly different micro-environments, and their distribution around an average time. The width of the distribution is extremely sensitive to the heterogeneity of the medium and a great deal of information can be thus obtained

out of it. Therefore, the complexation with magnesium cations proved as a valuable strategy to pull the drugs out of the hydrophobic matrix of the gel, being able to induce a controlled release of the active species against the bacteria, just like what was previously observed in the case of the cationic pDoTABr micelles.[40] These findings, gained by means of "state of the art" spectroscopic techniques and a careful analysis of the data acquired, revealed the potentiality of the pDoAO hydrogel as a drug vehicle for the tetracycline molecules and hopefully for other drugs.

Acknowledgements

Notes and references

ª Department of Chemistry, Biology and Biotechnology and Centre of Excellence on Nanostructured Innovative Materials (CEMIN) University of Perugia, via Elce di Sotto 8, 06123 Perugia (Italy).

1   A. S. Hoffman, *Adv. Drug Deliv. Rev.*, 2012, **64**, 13-23.

2   T. R. Hoare and D. S. Kohane, *Polymer*, 2008, **49**, 1993-2007.

3   L. Chen, J. Wu, L. Yuwen, T. Shu, M. Xu, M. Zhang and T. Yi, *Langmuir Lett.*, 2009, **25**, 8434-8438.

4   A. Baral, S. Roy, A. Dehsorkhi, I. W. Hamley, S. Mohapatra, S. Ghosh and A. Banerjee, *Langmuir*, 2014, **30**, 929-936.

5   J. Nanda, A. Biswas and A. Banerjee, *Soft Matter*, 2013, **9**, 4198-4208.

6   X. Li, J. Li, Y. Gao, Y. Kuang, J. Shi and B. Xu, *J. Am. Chem. Soc.,* 2010, **132**, 17707-17709.

7   J. Naskar, G. Palui, A. Banerjee, *J. Phys. Chem. B,* 2009, **113**, 11787-11792.

8   J. Li, X. Li, Y. Kuang, Y. Gao, X. Du, J. Shi and B. Xu, *Adv. Healthcare Mater.,* 2013, **2**, 1586-1590.

9   H. Rehage and H. Hoffmann, *J. Phys. Chem.*, 1988, **92**, 4712–4719.

10 F. Kern, P. Lemarechal, S. J. Candau and M. E. Cates, *Langmuir*, 1992, **8**, 437–440.

11 P. A. Hassan, S. J. Candau, F. Kern and C. Manohar, *Langmuir*, 1998, **14**, 6025–6029.

12 S. R. Raghavan, G. Fritz and E. W. Kaler, *Langmuir*, 2002, **18**, 3797–3803.

13 T. Shikata, M. Shiokawa and S.-I. Imai, S.-I., *J. Colloid Interface Sci.*, 2003, **259**, 367–373.

14 E. Sapelli, T. A. S. Brandão, H. D. Fiedler and F. Nome, *J. Colloid Interface Sci.*, 2007, **314**, 214-222.

15 S. J. George and A. Ajayaghosh, *Chem. Eur. J.*, 2005, **11**, 3217–3227.

16 M. J. Boerakker, N. E. Botterhuis, P. H. Bomans, P. M. Frederik, E. M. Meijer, R. J. Nolte and N. A. Sommerdijk, *Chem. Eur. J.*, 2006, **12**, 6071–6080.

17 X. Zhang, Z. Chen and F. Würthner, *J. Am. Chem. Soc.*, 2007, **129**, 4886–4887.

18 A. Ajayaghosh, P. Chithra, R. Varghese and K. P. Divya, *Chem. Commun.*, 2008, 969–971.

19 W. Cai, G. T. Wang, Y. X. Xu, X. K. Jiang and Z. T. Li, *J. Am. Chem. Soc.*, 2008, **130**, 6936–6937.

20 E. Szajdzinska-Pietek and S. Schlick, *Langmuir*, 1994, **10**, 2188-2196.

21 S. K. Pal, D. Sukul, D. Mandal, S. Sen and K. Bhattacharyya, *J. Phys. Chem. B*, 2000, **104**, 2613-2616.

22 L. Brinchi, R. Germani, P. Di Profio, L. Marte, G. Savelli, R. Oda and D. Berti, *J. Colloid Interface Sci.*, 2010, **346**, 100-106.

23 A. Di Crescenzo, L. Bardini, B. Sinjari, T. Traini, L. Marinelli, M. Carraro, R. Germani, P. Di Profio, S. Caputi, A. Di Stefano, M. Bonchio, F. Paolucci and A. Fontana, *Chem. Eur. J.*, 2013, **19**, 16415-16423.

24 M. Hrubý, Č. Koňák and K. Ulbrich, *J. Control. Release*, 2004, **103**, 137-148.

25 Y. Bae, W.-D. Jang, N. Nishiyama, S. Fukushima and K. Kataoka, *Mol. Biosyst.*, 2005, **1**, 242-250.

26 R. M. Sawant, J. P. Hurley, S. Salmaso, A. Kale, E. Tolcheva, T. S. Levchenko and V. P. Torchilin, *Bioconjugate Chem.*, 2006, **17**, 943-949.

27 D. Schmaljohann, *Adv. Drug Deliv. Rev.*, 2006, **58**, 1655-1670.

28 W. Chen, F. Meng, R. Cheng, and Z. Zhong, *J. Control. Release*, 2010, **142**, 40-46.

29 I. Chopra and M. Roberts, *Microbiol. Mol. Biol. Rev.*, 2001, **65** , 232-260.

30 M. O. Griffin, E. Fricovsky, G. Ceballos and F. Villarreal, *Am. J. Physiol.*, 2010, **299**, C539-C548.

31 F. Bahrami, D. L. Morris and M. H. Pourgholami, *Mini-Reviews in Medicinal Chemistry*, 2012, **12**, 44-52.

32 M. O. Schmitt, S. Schneider and M. L. Nelson, *Z. Phys. Chem.*, 2007, **221**, 235-271.

33 N. E. Rigler, S. P. Bag, D. E. Leyden, J. L. Sudmeier and C. N. Reilley, *Anal. Chem.*, 1965, **37**, 872-875.

34 B. Carlotti, D. Fuoco and F. Elisei, *Phys. Chem. Chem. Phys.*, 2010, **12**, 15580-15591.

35 M. O. Schmitt and S. Schneider, *PhysChemComm*, 2000, **3**, 42–55.

36 S. Schneider, G. Brehm, M. Schmitt, C. Leypold, P. Matousek and M. Towrie, *Lasers for Science Facility Programme—Chemistry Central Laser Facility Annual Report*, 2001/2002.

37 S. Schneider, M. O. Schmitt, G. Brehm, M. Reiher, P. Matousek and M. Towrie, *Photochem. Photobiol. Sci.*, 2003, **2**, 1107–1117.

38 B. Carlotti, A. Cesaretti and F. Elisei, *Phys. Chem. Chem. Phys.,* 2012, **14**, 823-834.

39 A. Cesaretti, B. Carlotti, C. Clementi, R. Germani and F. Elisei, *Photochem. Photobiol. Sci.*, 2014, **13**, 509-520.

40 A. Cesaretti, B. Carlotti, P. L. Gentili, C. Clementi, R. Germani and F. Elisei, *J. Phys. Chem. B*, 2014, **118**, 8601-8613.

41 L. Goracci, R. Germani, G. Savelli and D. M. Bassani, *ChemBioChem*, 2005, **6**, 197-203.

42 A. Romani, C. Clementi, C. Miliani, B. G. Brunetti, A. Sgamellotti and G. Favaro, *Appl. Spectrosc.*, 2008, **62**, 1395–1399.

43 B. Carlotti, R. Flamini, A. Spalletti, A. Marrocchi and F. Elisei, *ChemPhysChem,* 2012, **13**, 724-735.

44 A. Barbafina, L. Latterini, B. Carlotti and F. Elisei, *J. Phys. Chem. A*, 2010, **114**, 5980-5984.

45 A. Barbafina, M. Amelia, L. Latterini, G. G. Aloisi and F. Elisei, *J. Phys. Chem. A*, 2009, **113**, 14514-14520.

46 Copyright © 2009, J. Snellenburg, VU University Amsterdam; http://glotaran.org/

47 I. H. M. van Stokkum, D. S. Larsen and R. van Grondelle, *Biochim. Biophys. Acta*, 2004, **1657**, 82-104.

48 P. J. Steinbach, R. Ionescu and C. R. Matthews, *Biophys. J.*, 2002, **82**, 2244-2255.

49 P. J. Steinbach, *J. Chem. Inf. Comput. Sci.*, 2002, **42**, 1476-1478.

50 M. Penconi, P. L. Gentili, G. Massaro, F. Elisei and F. Ortica, *Photochem. Photobiol. Sci.*, 2014, **13**, 48-61.

51 P. L. Gentili, C. Clementi and A. Romani, *Appl. Spectrosc.*, 2010, **64**, 923–929.

52 C. R. Stephen, K. Murai, K. J. Burning and R. B. Woodward, *J. Am. Chem. Soc.*, 1956, **78**, 4155-4158.

53 D. Newton and R. Kluza, *Drug Intelligence and Clinical Pharmacy*, 1978, **12**, 546-554.

54 A. Sanz-Medel, R. F. de la Campa and J. I. G. Alonso, *Analyst*, 1987, **112**, 493-497.

55 A. Rei, G. Hungerford, M. Belsley, M. I. Ferreira and P. Schellenberg, *Int. J. Spectrosc.*, 2012, **2012**, ID 271435.

56 R. Jimenez, G. R. Fleming, P. V. Kuman, M. Maroncelli, *Nature*, 1994, **369**, 471−473.

57 S. A. Giannos, S. Dinh, B. Berner, *J. Pharm. Sci.*, 1995, **84**, 539−543.

58 P. L. Gentili, *RSC Advances*, 2013, **3**, 25523−25549.